Journal of Contaminant Hydrology 171 (2014) 12–21

Contents lists available at ScienceDirect

Journal of Contaminant Hydrology

journal homepage: www.elsevier.com/locate/jconhyd

Reaction front formation in contaminant plumes

Laura B. Cribbin [a], Henry F. Winstanley [a,*], Sarah L. Mitchell [a], Andrew C. Fowler [a,b], Graham C. Sander [b,c]

[a] MACSI, University of Limerick, Limerick, Ireland
[b] OCIAM, University of Oxford, Oxford, UK
[c] School of Civil and Building Engineering, Loughborough University, Loughborough, UK

ARTICLE INFO

Article history:
Received 28 April 2014
Received in revised form 26 September 2014
Accepted 6 October 2014
Available online xxxx

Keywords:
Bioremediation
Reactive transport
Terminal electron acceptors
Redox zonation
Reaction front
Mathematical model

ABSTRACT

The formation of successive fronts in contaminated groundwater plumes by subsoil bacterial action is a commonly accepted feature of their propagation, but it is not obviously clear from a mathematical standpoint quite how such fronts are formed or propagate. In this paper we show that these can be explained by combining classical reaction–diffusion theory involving just two reactants (oxidant and reductant), and a secondary reaction in which a reactant on one side of such a front is (re-)formed on the other side of the front via diffusion of its product across the front. We give approximate asymptotic solutions for the reactant profiles, and the propagation rate of the front.

© 2014 Published by Elsevier B.V.

1. Introduction

The motivation for modelling and simulating groundwater contaminant transport and degradation is clear and compelling. Groundwater contaminants from both historical and current human activity are ubiquitous in the developed and developing world. Human and environmental risks arise wherever these contaminants enter surface waters or abstraction wells. Site data is limited to spatially sparse datasets; data gathering costs are significant and remedial intervention costs are high and generally prohibitive. Hence quantitative predictions of contaminant concentrations are of great importance in assessing necessary actions. However, there are limitations on the accuracy and reliability of predictive models: the heterogeneity of natural media introduces uncertainties, and though the physico-chemical processes are relatively well understood, knowledge of microbial processes and rates is limited.

Microbially-mediated reactions are the dominant process in degradation of many groundwater contaminants. In particular, a wide range of common organic (e.g. petrochemicals, solvents, coal tars) and inorganic (e.g. ammonia) groundwater contaminants are degraded by respirative microbiota, whose respiration is effectively an overall redox reaction between these contaminants as electron donors and a terminal electron acceptor (TEA) sourced from the local environment. The availability of TEAs and thermodynamic viability of TEA-donor redox couples depends on spatial location and chemical environment, but a typical range can include dissolved oxygen, nitrate, manganese (IV) and iron (III) minerals, sulphate, and carbon dioxide (in approximate order of oxidant strength).

The paradigm of redox zonation due to microbially mediated reactions in groundwater and aquatic sediments is well-engrained in the literature (cf. Chapelle, 2001; Christensen et al., 2000; Froelich et al., 1979). In its barest form, the principle is that microbes exploiting higher energy yield reactions will tend to outcompete others and dominate the local electron flux (i.e. overall reaction rate). As a result, a spatial sequence of more-or-less distinct zones forms in which each zone is dominated by

* Corresponding author.
E-mail address: henry.winstanley@ul.ie (H.F. Winstanley).

http://dx.doi.org/10.1016/j.jconhyd.2014.10.006
0169-7722/© 2014 Published by Elsevier B.V.

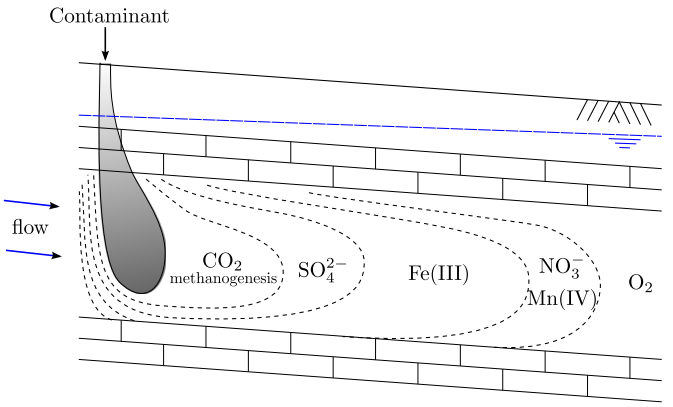

Fig. 1. Schematic propagation of a contaminant plume, and the zones where the successive terminal electron acceptors operate, separated by a sequence of reaction fronts.

a specific TEA process until that TEA is depleted, and the next zone is dominated by the next most reactive available TEA in sequence, as depicted in Fig. 1. Relative to the redox zone width, the transitions between redox zones often appear to occur over relatively short distances of order 1 m or less in contaminant plumes suggesting that at the field scale they may be thought of as reaction fronts.

This simple conceptual model focussing on TEA processes tacitly assumes that the dominant electron donors have relatively constant concentrations across the redox zones, whether occurring as the primary contaminant, or as simpler species resulting from microbial fermentation, such as hydrogen and acetate. Interestingly, this conflicts with what one might expect based on standard mathematical models of reaction fronts. Generally, when two diffusible reagents are supplied from opposite sides of a domain and the reaction rate is fast relative to transport, the solution is a reaction front with a distinct reaction zone flanked by diffusion-dominated zones in which negligible reaction occurs. Crucially, both reagents are 'taken out' by the front so that their concentrations are asymptotically small on the side away from their supply, and the reaction is effectively confined to the narrow reaction zone where both reagents are present (e. g., Gálfi and Rácz, 1988; Hagan et al., 1985). The position of the reaction front reflects the reaction stoichiometry and rate of supply of each reagent (Nambi et al., 2003).

The aim of the current paper is to reconcile the transition between successive redox zones in a contaminant plume with standard mathematical modelling of reaction fronts. We do this by building a simplified model of just the dominant reactions in a single such transition in order to illustrate the mathematical structure. The extension to multiple transitions is then largely a straightforward exercise.

A number of other papers have addressed the issue of modelling reaction fronts. Gálfi and Rácz (1988) (see also Chu et al., 2005) effectively solved the reaction front dynamics of the reaction $A + B \rightarrow C$ at large times; their work was partly motivated by the phenomenon of Liesegang rings, which were modelled in detail by Keller and Rubinow (1981) and Feeney et al. (1983). Taitelbaum et al. (1992) studied a two-component reaction–diffusion front, focussing interest on the rate of movement of the reaction front. Their analysis was valid for early times, and was later elaborated by Koza and Taitelbaum (1996). Sinder and Pelleg (1999) extended these results to the case of a reversible reaction. Our present interest, however, is in the large time limit where the reactions are fast, and the results of Gálfi and Rácz (1988) are the most relevant.

Consideration of reaction fronts in contaminant plumes has been a focus of a number of papers. Gutierrez-Neri et al. (2009) considered fringe and core degradation, but assumed an instantaneous reaction between electron acceptor and electron donor at the fringe. A number of papers consider a simple two species reaction (between for example CH_2O and O_2) with associated growth of biomass, and give various analytic and numerical approximations to the propagation of the front (Cirpka, 2010; Keijzer et al., 1998); some study the front propagation as that of a travelling wave (Keijzer et al., 1999), where the front can be oscillatory (Murray, 2002; Oya and Valocchi, 1997); and a number of researchers prove mathematical results (Beck et al., 2006; Ai, 2007; Xin and Hyman, 2000). Other studies using numerical solutions of similar kinetic formulations include those of Abrams and Loague (2000a,b), Wang and Van Cappellen (1996), MacQuarrie and Sudicky (2001), Thullner et al. (2005), and Rolle et al. (2008).

Our approach is very different in aim and scope both to the more analytic papers referred to above, where the dynamics of the simplest (two species plus biomass) model is studied, and also to the standard approach of using a numerical simulation package to solve a highly detailed reactive transport system. Many good examples of such packages exist (such as PHREEQC, PHAST, HYDRUS 2D/3D, MIN3P, ORCHESTRA), each with its particular approach and emphasis. The typical complexity of the underlying models (and hence parameterisation) of these packages provides ease of application in diverse settings, but often contrasts with the treatment of biotic reaction rates and microbial population interactions due to the inherent uncertainties and site specificity in these. And yet, the redox zonation paradigm hinges on the emergence of a dominant metabolic type through population competition, so for our purposes a greatly simplified model appears warranted and can have the benefit of providing greater mechanistic insight. For simplicity we base our study on the one-dimensional kinetic model of Hunter et al. (1998), whose numerical solutions provide indication of front formation.

The resolution to the apparent conflict between the reaction front paradigm and the persistence of the primary electron donor across the front lies in the presence of secondary

reactions between the dominant TEA of one redox zone and the reduced product of the (less potent) dominant TEA in the adjacent zone. It is these species – and not the primary electron donor – which are effectively 'taken out' by the reaction front. The structure of this transition is our focus.

Despite the familiarity of the idea of reaction fronts, there seems to be little that has been done in the way of understanding how they occur in the specific context of contaminated groundwater.

Dewynne et al. (1993) provided a simplified asymptotic analysis of paired redox fronts due to uranium mediation of iron pyrite oxidation in iron-rich uranium deposits, giving an analytical expression for the fronts' propagation speed. Ham et al. (2004) and Liedl et al. (2005) modelled the progression of a binary reaction front caused by advection of a plume of one reactant into a region of initially uniform concentration of another reactant, assuming instantaneous reaction so that both reactants were eliminated at the front position. Cirpka and Valocchi (2007, 2009) and Cirpka (2010) extended this analysis by considering a fast but finite biologically-controlled reaction rate and, by implication, a narrow front region rather than a discrete interface. Solutions either side of the reaction front were reconciled by assuming the front position coincided with that for an instantaneous reaction rather than by asymptotic matching.

Our paper proceeds as follows. In Section 2, we briefly review the classical one-dimensional model of the diffusion of two reactants towards a reaction front, and then we outline the model of Hunter et al. (1998). In Section 3 we analyse a simple reduction of this model so as to show how front formation and propagation can be simply explained. The conclusions follow in Section 4.

2. Redox zonation

The archetypal respiration reaction is

$$CH_2O + O_2 \rightarrow CO_2 + H_2O + \text{energy}, \tag{2.1}$$

where CH_2O represents a generic organic electron donor and oxygen acts as the electron acceptor, more explicitly shown by the paired oxidation and reduction half-reactions:

$$\begin{aligned} CH_2O + H_2O &\rightarrow CO_2 + 4H^+ + 4e^-, \\ O_2 + 4H^+ + 4e^- &\rightarrow 2H_2O. \end{aligned} \tag{2.2}$$

The essential characteristic of microbial respiration reactions is the diversity of such redox reactions that can be exploited to harvest energy, both by different organisms and by adaptation. Thus within a soil or aquifer material, different chemical species participate as electron donor or acceptor across both space and time.

For a single reaction such as Eq. (2.1), a simple paradigm for modelling this situation is the reaction of two chemicals A and B which are suddenly brought into contact, and react to form a product C:

$$\nu_A A + \nu_B B \xrightarrow{k} \nu_C C, \tag{2.3}$$

where ν_K are stoichiometric constants. For example, we might think of A as oxygen and B as organic carbon, and we might think of C as carbon dioxide. Of course, in reality such metabolic reactions have multiple intermediate steps catalysed by enzymes, and this determines the overall reaction kinetics. Let us suppose this reaction occurs on a one-dimensional domain with spatial coordinate x and that each species is in aqueous form. We suppose that initially the corresponding concentrations satisfy $[A] = a_0$ in $x < 0$ and $[A] = 0$ in $x > 0$, while $[B] = b_0$ in $x > 0$ and $[B] = 0$ in $x < 0$. Also, $[C] = 0$ everywhere initially. Approximate solutions of versions of this problem have been given by Gálfi and Rácz (1988) and Feeney et al. (1983), for example, and are illustrated in Fig. 2. We can define a dimensionless parameter

$$\Lambda = \frac{k b_0 l^2}{D}, \tag{2.4}$$

where we take all the stoichiometric constants ν_K to be one, l is a suitable length scale, and D is the dispersion coefficient. The case of interest is when the reactions are fast, and then $\Lambda \gg 1$; in this case the solution effectively consists of distinct subdomains: a thin inner reaction zone near a reaction front at $x = x_f$ (where $x_f(t)$ must be calculated), surrounded on both sides by an outer, diffusive zone where there is in effect no reaction. On the basis that $\Lambda \gg 1$, asymptotic approximations to the solution can be constructed analytically by solving appropriately-scaled equations in each subdomain to a leading order of approximation and then requiring that the solutions match across transitions between subdomains (Cribbin, 2013). Fig. 2 shows a snapshot of the numerical solution which illustrates the above description. Pore water concentration profiles in borehole data and numerical simulations commonly show similar sharp drop-offs with an absence of reactant on one side of the front.

Now we place our discussion of front dynamics in the context of sequential reactions in a redox hierarchy, as modelled by Hunter et al. (1998). We also extend the analysis of the reaction front to include advection, requiring a more complex asymptotic solution structure around the front.

Hunter et al. (1998) proposed a one-dimensional kinetic model of microbially-driven redox chemistry of subsurface environments. Various primary and secondary redox reactions are considered along with other non-redox reactions which will not be discussed here. For each dissolved chemical species i, Hunter et al. (1998) write a mass conservation equation in the form

$$\frac{\partial C_i}{\partial t} = \frac{\partial}{\partial x}\left(D\frac{\partial C_i}{\partial x}\right) - \frac{\partial (v C_i)}{\partial x} + R_i, \tag{2.5}$$

where x is in the direction of groundwater flow, C_i is the local concentration of component i, D is the dispersion coefficient, v is the flow velocity and R_i is the net rate of production by local reactions. Solid phase species are assumed immobile and evolve in response to local reaction terms alone.

A source of dissolved organic carbon (DOC) at $x = 0$ provides the primary electron donor in a plume downstream ($x \geq 0$). The overall rate of DOC degradation occurs through the sequential depletion of oxygen, nitrate, and so on, and is assumed here to follow first order kinetics, since this was also the assumption of Hunter et al. (1998):

$$R_{DOC} = k_{DOC}[CH_2O], \tag{2.6}$$

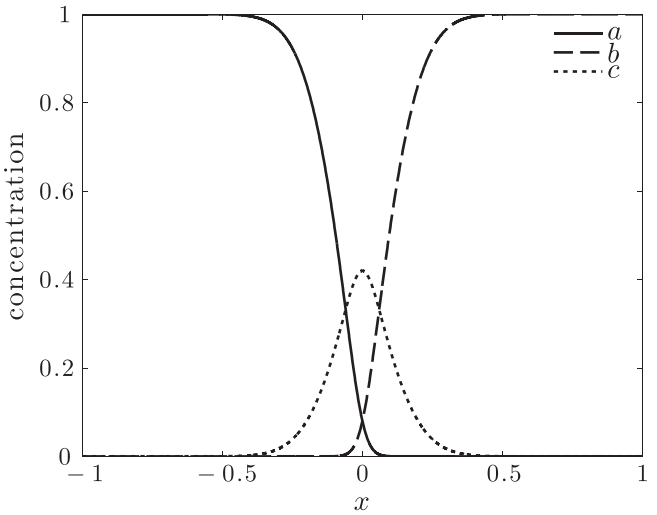

Fig. 2. Profiles of [A]/a_0, [B]/b_0 and [C]/a_0 for $a_0 = b_0$ and $\Lambda = 10^4$ at time $t = 0.001$.

where k_{DOC} is the reaction rate constant. Under the stoichiometry of Eq. (2.2)$_1$, this effectively defines an overall electron flow $R_e = 4R_{DOC}$ which Hunter et al. (1998) allocate among the various TEA processes according to a hierarchy in which each primary half-reaction R_j involving the jth TEA receives a fraction h_j of the electron flow as

$$R_j = \frac{h_j}{e_j} R_e, \tag{2.7}$$

where e_j is the electron transfer stoichiometry of the half-reaction. Ranking the TEAs in order of decreasing energy yield, the relative fractions h_j are given as

$$h_1 = \min\left(1, \frac{[\mathrm{TEA}_1]}{[\mathrm{TEA}_1^*]}\right), \tag{2.8}$$

$$h_j = \min\left(1, \frac{[\mathrm{TEA}_j]}{[\mathrm{TEA}_j^*]}\right) \prod_{i=1}^{j-1} \left(1 - \frac{[\mathrm{TEA}_i]}{[\mathrm{TEA}_i^*]}\right)_+ \quad \text{for} \quad j = 2, 3, 4, \ldots \tag{2.9}$$

where a limiting concentration $[\mathrm{TEA}_i^*]$ is assumed for each TEA. Thus at any location and time, a particular TEA half-reaction only occurs if all higher-yielding TEAs are sufficiently depleted.

Hunter et al. (1998) used this as a framework for numerical simulations. We choose to take a more detailed analytical look at the transition between the first two redox zones in their TEA hierarchy (outermost in the plume), considering the oxidation of organic carbon paired with only the TEA processes[1]

$$\begin{aligned} &O_2 + 4H^+ + 4e^- \rightarrow 2H_2O, \\ &MnO_2 + 4H^+ + 2e^- \rightarrow Mn^{2+} + 2H_2O, \end{aligned} \tag{2.10}$$

and, critically, the single secondary reaction

$$Mn^{2+} + \frac{1}{2}O_2 + H_2O \xrightarrow{k} MnO_2 + 2H^+, \tag{2.11}$$

where k is a rate constant. In this secondary redox reaction, $Mn^{2+}_{(aq)}$ diffusing from the site of its production to the oxic zone is reoxidised there by O_2. In a sharp transition between redox zones, the reaction front analysis above would suggest that both the dominant TEA (O_2) and primary electron donor (DOC) would be 'taken out' by the front. We posit instead that a reaction front is formed in which the dominant TEA (O_2) and the *secondary* electron donor Mn^{2+} are mutually annihilated, thus admitting the presence of DOC on both sides of the front.

To proceed, we denote the concentration of the reactants by $g = [\mathrm{TEA}_1] = [O_2]$, $p = [Mn^{2+}]$, $m = [\mathrm{TEA}_2] = [MnO_2]$ and $c = [CH_2O]$. A comment on the meaning of the solid phase concentration m is necessary, although in writing Eq. (2.12) below we are simply following Hunter et al.'s (1998) prescription. If p measures aqueous concentration as moles per litre of the subsurface aquifer (that is the molar concentration divided by the porosity), then so also does m. However, because m is a solid phase, its dissolution rate R_2 below must depend on the specific available surface area of MnO_2. In general this will be some function of m, but the complexity of this dependence is ignored in our model. The evolution of each species is described by

$$\begin{aligned} g_t &= Dg_{xx} - vg_x - R_1 - \frac{1}{2}kpg, \\ p_t &= Dp_{xx} - vp_x + R_2 - kpg, \\ c_t &= Dc_{xx} - vc_x - k_{DOC}c, \\ m_t &= -R_2 + kpg, \end{aligned} \tag{2.12}$$

where R_i is the rate of production of species i and is given by

$$\begin{aligned} R_1 &= k_{DOC}\, cS_1, \quad S_1 = \min\left(1, \frac{g}{g^*}\right), \\ R_2 &= 2k_{DOC}\, cS_2, \quad S_2 = \min\left(1, \frac{m}{m^*}\right)\left(1 - \frac{g}{g^*}\right)_+, \end{aligned} \tag{2.13}$$

[1] We note that nitrate reduction commonly coincides with or precedes the zone of MnO_2 reduction. For simplicity we ignore the complications of nitrogen speciation and reactions in the current analysis, and assume nitrate is absent.

where an asterisk denotes the limiting concentration of the TEA.

We choose boundary conditions similar to those of Hunter et al. (1998), with a constant concentration source at $x = 0$:

$$\begin{aligned} &g(0,t) = 0, \quad c(0,t) = c_0, \quad p_x(0,t) = 0, \\ &g_x(l,t) = 0, \quad c_x(l,t) = 0, \quad p(l,t) = 0, \end{aligned} \tag{2.14}$$

and we choose initial conditions in which the native aquifer is aerobic and pristine with some known MnO_2 mineral content:

$$g(x,0) = g_0, \quad c(x,0) = p(x,0) = 0, \quad m(x,0) = m_0. \tag{2.15}$$

2.1. Nondimensionalisation

The model is nondimensionalised by setting

$$t \sim \frac{l}{v}, \quad x \sim l, \quad g \sim g_0, \quad p \sim p_0 = \frac{2k_{\mathrm{DOC}} c_0 l}{v}, \quad c \sim c_0, \quad m \sim m_0, \tag{2.16}$$

to give the dimensionless model

$$\begin{aligned} g_t &= \frac{1}{Pe} g_{xx} - g_x - \lambda_1 c S_1 - \Lambda p g, \\ p_t &= \frac{1}{Pe} p_{xx} - p_x + c S_2 - \lambda_2 \Lambda p g, \\ c_t &= \frac{1}{Pe} c_{xx} - c_x - \lambda_3 c, \\ m_t &= -\kappa \lambda_1 c S_2 + \kappa \Lambda p g, \end{aligned} \tag{2.17}$$

where S_i in Eq. (2.13) can be written as

$$\begin{aligned} S_1 &= \min\,(1, \alpha g), \\ S_2 &= \min\,(1, \beta m)(1 - \alpha g)_+. \end{aligned} \tag{2.18}$$

The nondimensional parameters are defined as

$$\begin{aligned} &Pe = \frac{vl}{D}, \quad \lambda_1 = \frac{k_{\mathrm{DOC}} c_0 l}{v g_0}, \quad \lambda_2 = \frac{1}{\lambda_1} = \frac{v g_0}{k_{\mathrm{DOC}} c_0 l}, \\ &\lambda_3 = \frac{k_{\mathrm{DOC}} l}{v}, \quad \Lambda = \frac{k k_{\mathrm{DOC}} c_0 l^2}{v^2}, \quad \kappa = \frac{2 g_0}{m_0}, \\ &\alpha = \frac{g_0}{g^*}, \quad \beta = \frac{m_0}{m^*}, \end{aligned} \tag{2.19}$$

and, using Table 1, have numerical values

$$\begin{aligned} &Pe \approx 100, \quad \lambda_1 \approx 1.8, \quad \lambda_2 \approx 0.56, \quad \lambda_3 \approx 0.1, \\ &\Lambda \approx 1.4 \times 10^5, \quad \kappa \approx 20, \quad \alpha \approx 10, \quad \beta \approx 0.3; \end{aligned} \tag{2.20}$$

Λ is a suitable Damköhler number (Keijzer et al., 1998).

The nondimensional boundary conditions are

$$\begin{aligned} &g = 0, \quad c = 1, \quad p_x = 0 \quad \text{at} \quad x = 0, \\ &g_x = 0, \quad c_x = 0, \quad p = 0 \quad \text{at} \quad x = 1, \end{aligned} \tag{2.21}$$

and the initial conditions become

$$g = m = 1, \quad c = p = 0 \quad \text{at} \quad t = 0. \tag{2.22}$$

Fig. 3 shows the numerical solution of Eq. (2.17) plotted at (dimensionally) $t = 5$ and 10 years. Solutions were obtained in MATLAB using the method of lines. The Mn^{2+} and oxygen profiles are seen to be mutually removed in a manner similar to a reaction front which migrates in time.

Table 1
Values of constants as used by Hunter et al.'s (1998) leachate contaminated aquifer case.

Parameter	Value
c_0	3 mM
D	40 $m^2\ y^{-1}$
g_0	0.2 mM
g^*	2×10^{-5} M
k	$10^7\ M^{-1}\ y^{-1}$
k_{DOC}	$3 \times 10^{-3}\ y^{-1}$
l	400 m
m_0	0.02 mmol dm^{-3}
m^*	0.06 mmol dm^{-3}
p_0	0.72 nM
v	10 m y^{-1}

3. Front formation

We are interested in providing some analytic insight into the way in which the front forms, by analogy with comparable studies for simple bimolecular reactions (Gálfi and Rácz, 1988); we also wish to demonstrate a method of solving the problem which avoids resolving the very thin reaction zones. To do this, we consider a simplified version of Eq. (2.17). The essence of front formation is captured in the reduced system for oxygen (g) and Mn^{2+} (p),

$$\begin{aligned} g_t &= \frac{1}{Pe} g_{xx} - g_x - \lambda_1 c S_1 - \Lambda p g, \\ p_t &= \frac{1}{Pe} p_{xx} - p_x + c S_2 - \lambda_2 \Lambda p g, \end{aligned} \tag{3.1}$$

which differs from the basic reaction front model of Section 2 through the fact that the manganese ions which take out the oxygen at the front are themselves the product of a separate reaction, the reduction of manganese dioxide. Hence, importantly, there is a source term in the p equation which cannot be ignored. We take boundary and initial conditions for Eq. (3.1) as for the complete model, thus from Eqs. (2.21) and (2.22),

$$\begin{aligned} &g = 0, \quad p_x = 0 \quad \text{at} \quad x = 0, \\ &g_x = 0, \quad p = 0 \quad \text{at} \quad x = 1, \\ &g = 1, \quad p = 0 \quad \text{at} \quad t = 0. \end{aligned} \tag{3.2}$$

We examine the asymptotic structure of solutions, based on the parameter relations $\Lambda \gg 1$, $Pe \gg 1$. The solution domain can be partitioned into a number of regions: the reaction layer, a thin region around the reaction front $x = x_f(t)$ where the O_2–Mn^{2+} reaction occurs; diffusion-dominated layers on each side, in which the reactants are transported to the reaction front; and advection-dominated outer layers on each side in which both the front reaction and diffusion are small.

For convenience, we take c to be constant and $O(1)$. The prescriptions of S_1 and S_2 are given in Eq. (2.18). Since from Fig. 3, $m \sim O(1)$, it seems $\min(1, \beta m) = \beta m$, and for simplicity we take $m = 1$, so that

$$\begin{aligned} S_1 &= 1 - f(g) \\ S_2 &= \beta f(g), \end{aligned} \tag{3.3}$$

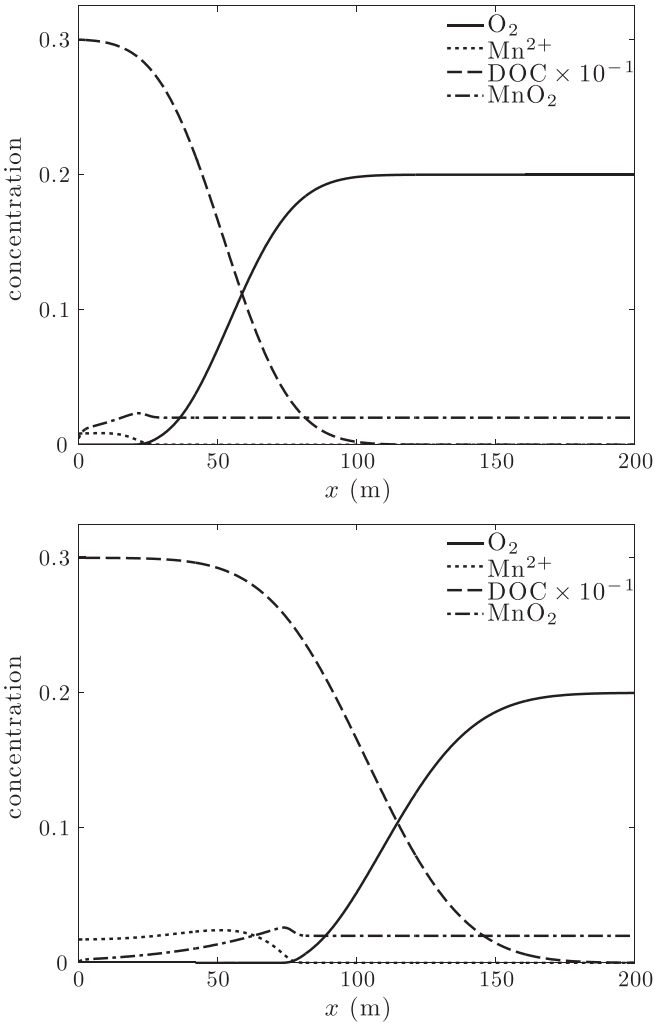

Fig. 3. Numerical solution of Eq. (2.17) showing the concentration profiles of dissolved O_2 ($\propto g$), Mn^{2+} ($\propto p$), DOC ($\propto c$) (all mM) and MnO_2 ($\propto m$) (mmol dm^{-3}) at 5 years (top) and 10 years (bottom). The reaction front between O_2 and MnO_2 is sharp due to the largeness of the parameter Λ, which can be taken as meaning a large reaction rate k.

where in Eq. (2.18) $f(g) = [1 - \alpha g]_+$, but in our illustrations we choose

$$f(g) = \exp(-ag), \tag{3.4}$$

where a value $a = 40$ gives a function reasonably akin to Eq. (2.18) with $\alpha = 10$. In particular, we have

$$\begin{aligned} &S_1 = 0, \quad S_2 = \beta, \quad g \ll \frac{1}{a}, \\ &S_1 = 1, \quad S_2 = 0, \quad g \gg \frac{1}{a}. \end{aligned} \tag{3.5}$$

We now investigate the solution regions in turn. It follows from the assumption that $m = 1$ and c is constant that our analytic solutions will be only qualitatively similar to Fig. 3.

3.1. Advective outer layers

In $0 < x < x_f$, we anticipate that the oxygen has been removed, $g \approx 0$, so that the fast reaction terms proportional to Λpg are zero. We ignore the diffusive terms on the basis that $Pe \gg 1$. The leading order solution of the p equation satisfying the no flux boundary condition is simply

$$p = \beta c(t - t^*), \quad x < x_f, \tag{3.6}$$

where the constant t^* is discussed further below. Similarly in $x > x_f$, we take $p = 0$, and solving the leading order equation for g yields

$$g = 1 - \lambda_1 ct. \tag{3.7}$$

Note that g remains positive as long as $t < t_0$, where

$$t_0 = \frac{1}{\lambda_1 c}, \tag{3.8}$$

after which the solution is terminated.

3.2. Diffusive layers

The reaction front is close to the advection front at $x = t$, and we write

$$x = t + \frac{X}{\sqrt{Pe}}, \quad x_f = t + \frac{X_f}{\sqrt{Pe}}. \tag{3.9}$$

The diffusive layer equations are thus (the reactive terms being ignored)

$$\begin{array}{l} p_t = p_{XX} + \beta c, \quad g = 0, \quad X<X_f, \\ g_t = g_{XX} - \lambda_1 c, \quad p = 0, \quad X>X_f, \end{array} \tag{3.10}$$

and they satisfy the boundary (matching) conditions

$$\begin{array}{llll} p \to 0 & \text{as} \quad X \to X_f-, & g \to 0 & \text{as} \quad X \to X_f+, \\ p \to \beta c(t-t^*) & \text{as} \quad X \to -\infty, & g \to 1-\lambda_1 ct & \text{as} \quad X \to +\infty. \end{array} \tag{3.11}$$

X_f is the value of X at the front.

3.3. Reaction front

Let us define the gradients of the solutions of the diffusive layer at the reaction front as

$$-p_X|_{X_f-} = p', \quad g_X|_{X_f+} = g'. \tag{3.12}$$

As $X \to X_f$, it is therefore appropriate to rescale the variables in the reaction layer as

$$X = \varepsilon\xi, \quad p = \varepsilon P, \quad g = \varepsilon G, \tag{3.13}$$

and it follows from balancing the reaction and diffusion terms that we should choose

$$\varepsilon = \left(\frac{1}{\Lambda}\right)^{1/3} \ll 1. \tag{3.14}$$

At leading order, the equations take the form

$$G_{\xi\xi} = PG, \quad P_{\xi\xi} = \lambda_2 PG, \tag{3.15}$$

with matching conditions

$$\begin{array}{llll} G \to 0, & P \sim -p'\xi & \text{as} & \xi \to -\infty, \\ P \to 0, & G \sim g'\xi & \text{as} & \xi \to +\infty. \end{array} \tag{3.16}$$

Two integrations yield

$$P = \lambda_2 G - p'\xi, \tag{3.17}$$

from which (using Eq. (3.16)) it immediately follows that

$$p' = \lambda_2 g'. \tag{3.18}$$

If we write

$$G = A(\phi + \eta), \quad \xi = B\eta, \tag{3.19}$$

where

$$A = \frac{1}{\lambda_2}\left(\frac{p'}{2}\right)^{2/3}, \quad B = \left(\frac{2}{p'}\right)^{1/3}, \tag{3.20}$$

then ϕ satisfies

$$\phi'' = \phi^2 - \eta^2, \quad \phi \sim \pm\eta \quad \text{as} \quad \eta \to \pm\infty. \tag{3.21}$$

This equation also arises in the simple reaction front model, see Gálfi and Rácz (1988) or Cribbin (2013). The solution is symmetric and convex, with $\phi(0) \approx 0.87$.

3.4. Summary

The solution of the reaction–diffusion–advection model (Eq. (3.1)) has been reduced to the solution of the diffusive model (Eq. (3.10)). Our gain is that we do not need to resolve the thin reaction layer, its dynamics being captured by the extra free boundary condition (3.18) which determines X_f; but generally it requires a numerical solution. The diffusive model of Eqs. (3.10) and (3.11) can be written as follows; define

$$p = \beta ct - \lambda_2 u, \quad g = v - \lambda_1 ct; \tag{3.22}$$

then

$$u_t = u_{XX}, \quad X<X_f; \qquad v_t = v_{XX}, \quad X>X_f, \tag{3.23}$$

with

$$u \to \lambda_1 \beta ct^*; \qquad X \to -\infty; \qquad v \to 1; \qquad X \to +\infty; \tag{3.24}$$

(using the fact that $\lambda_1\lambda_2 = 1$), and

$$u_X = v_X, \quad u = \lambda_1 \beta ct, \quad v = \lambda_1 ct \quad \text{on} \quad X = X_f. \tag{3.25}$$

The simplest assumption is that $t^* = 0$, on the basis that the front starts at $x_f = 0$ and immediately moves forward into the domain. In this case, apparent initial conditions for the system would be

$$\left.\begin{array}{l} u = 0, \quad X<X_f, \\ v = 1, \quad X>X_f, \end{array}\right\} \quad \text{at} \quad t = 0. \tag{3.26}$$

In general this system requires numerical solution, but a particular simplification, which we use below, follows if $\beta = 1$; then u is the continuation of v, and the solution is simply

$$v = \frac{1}{2}\left[1 + \operatorname{erf}\left(\frac{X}{2\sqrt{t}}\right)\right] = 1 - \frac{1}{2}\operatorname{erfc}\left(\frac{X}{2\sqrt{t}}\right), \tag{3.27}$$

from which it follows that

$$x_f = t + \frac{X_f}{\sqrt{Pe}} = t + 2\left(\frac{t}{Pe}\right)^{1/2} \mathrm{erf}^{-1}[2\lambda_1 ct - 1]. \tag{3.28}$$

Note that $x_f \to \infty$ when $t = t_0$ as defined in Eq. (3.8), which is when the solution terminates in any case.

This approximation works fairly well, but the value of p is overestimated. The reason for this is apparent in Eq. (3.28), which shows that $x_f < 0$ for an initial time $t < t^* = \frac{T^*}{Pe}$ (and T^* increases mildly with Pe). Of course this cannot be. In reality there is a short start-up time of $O(\frac{1}{Pe})$ when the front is pinned to $x = 0$, and the appropriate condition for g is that $g = 0$ on $x = 0$. In this initial phase the slope of g decreases, so that there is a waiting time t^* after which the front detaches (when g_x reaches zero).

3.5. The start-up problem

To deal with this issue, it is useful to define the small time and space coordinates

$$T = Pe\ t, \quad Y = Pe\ x. \tag{3.29}$$

Then the equations for u and v take the form

$$u_T + u_Y = u_{YY}, \quad Y < Y_f; \qquad v_T + v_Y = v_{YY}, \quad Y > Y_f, \tag{3.30}$$

and for large $T > T^*$ and large Pe, the boundary conditions are

$$\begin{aligned} &u = \frac{\lambda_1 \beta c T^*}{Pe} \quad \text{on} \quad Y = 0, \qquad v \to 1 \quad \text{as} \quad Y \to \infty, \\ &u_Y = v_Y, \quad u = \frac{\lambda_1 \beta c T}{Pe}, \quad v = \frac{\lambda_1 c T}{Pe} \quad \text{on} \quad Y = Y_f > 0, \quad T > T^*, \end{aligned} \tag{3.31}$$

but during the waiting time we have

$$\begin{aligned} &v = \frac{\lambda_1 c T}{Pe} \quad \text{on} \quad Y = 0, \\ &v_Y = 0 \quad \text{on} \quad Y = Pe, \\ &Y_f = 0, \quad T < T^*. \end{aligned} \tag{3.32}$$

The actual initial condition is then

$$v = 1 \quad \text{at} \quad t = 0, \quad Y > 0. \tag{3.33}$$

The value of T^* is determined by when v_Y reaches (approximately) 0 at $Y = 0$.

Again taking $\beta = 1$, we have $u = v$. The simple approximate solution (3.27) can be written in the form

$$v = 1 - \frac{1}{2}\mathrm{erfc}\left(\frac{Y - T}{2\sqrt{T}}\right), \tag{3.34}$$

but clearly does not satisfy the corrected boundary condition on $Y = 0$. To satisfy this, we amend Eq. (3.34) by taking

$$v = 1 - \frac{1}{2}\left(1 - \frac{\lambda_1 c T^*}{Pe}\right)\left[\mathrm{erfc}\left(\frac{Y - T}{2\sqrt{T}}\right) + e^Y \mathrm{erfc}\left(\frac{Y + T}{2\sqrt{T}}\right)\right], \tag{3.35}$$

which satisfies the equation and both boundary conditions. In terms of X and t, this is

$$v = 1 - \frac{1}{2}\left(1 - \frac{\lambda_1 c T^*}{Pe}\right) \times \left[\mathrm{erfc}\left(\frac{X}{2\sqrt{t}}\right) + e^{Pe\ x}\mathrm{erfc}\left(\sqrt{Pe\ t} + \frac{X}{2\sqrt{t}}\right)\right]. \tag{3.36}$$

Fig. 4 shows the asymptotic and numerical solution of g and p using the definition of v in Eq. (3.36), for values $Pe = 10^2$ and $\Lambda = 1.4 \times 10^5$. It can be seen that the approximate solution is essentially exact. This lends confidence to the use of the diffusive approximation in calculating front position. Direct comparison of this solution with Fig. 3 shows the location of the O_2—Mn^{2+} front in a similar position despite our coarse assumption of constant m.

The analytic approximation is based on the assumptions $Pe \gg 1$, $\Lambda \gg 1$. We have explored the sensitivity of the approximation to the size of the parameters, and find that the approximation is most sensitive to the value of Pe. While $Pe = 10^2$ gives an excellent approximation, even for $\Lambda = 1$ (!), the approximation becomes increasing inaccurate as Pe is reduced. At $Pe = 10$, it is still qualitatively accurate, but the accuracy is poor — perhaps unsurprisingly, since then $\frac{1}{\sqrt{Pe}} \approx 0.3$. Note that the achievement of the accuracy in Fig. 4 relies on an appropriate choice of T^*, which is done here by inspection; an analytic determination of T^* involves the analysis of the start-up problem.

Laboratory experimental work clearly shows that the concept of dispersivity gives an appropriate description of species transport in porous media, although its magnitude is affected by the presence of chemical reactions (Chiogna et al., 2010; Gramling et al., 2002); but at field scale, the detail of the magnitude of the dispersivity is less important, providing the Péclet number is large, as is commonly the case. The class of models we study should therefore be useful representations of field data, which commonly shows fronts of the type we discuss (Lerner et al., 2000; Smits et al., 2009), providing the issues of pore scale heterogeneity and bioavailability can be overcome in order to provide realistic field scale reaction rates and dispersivities.

4. Conclusions

The common cartoon of a spreading groundwater plume of contaminants as illustrated in Fig. 1, and as can be found in various descriptions, e. g., Chapelle (2001, Fig. 10.7), Gutierrez-Neri et al. (2009, Fig. 1) indicates a succession of reaction fronts as the hierarchy of terminal electron acceptors is successively depleted. That these fronts are indeed sharp is also suggested by borehole data, which commonly show abrupt termination of single species concentration profiles (Fowler et al., 2014, Fig. 1; Lerner et al., 2000, Fig. 2; Smits et al., 2009, Fig. 2). And yet, the classical picture of a reaction front, as shown here in Fig. 2, requires the disappearance of *two* reactants at a front. We have made a series of efforts to find a reaction scheme which can allow the disappearance of a single species at a front, without avail. The question then arises, if a TEA disappears at a front, what is the presumed other reactant involved?

In this paper, we have shown that a classical reaction front analysis allows us to explain the dynamics of contaminant

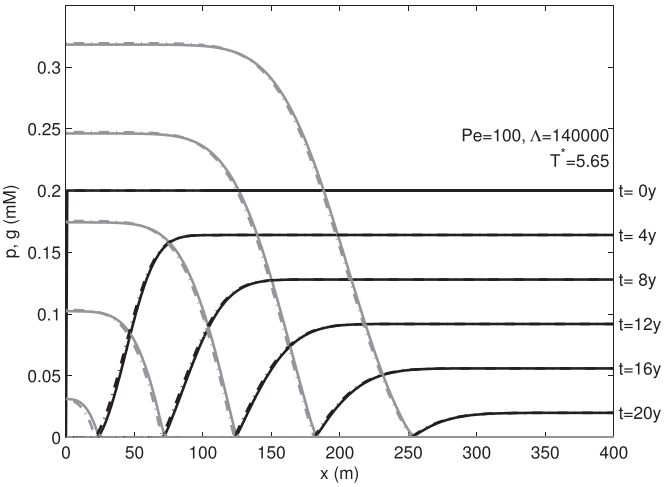

Fig. 4. Dimensional numerical (solid) and asymptotic (dashed) solutions of (3.1) showing the concentration profiles of dissolved O_2 (black) and Mn^{2+} (grey) at a sequence of values of time of 0, 4, 8, 12, 16, 20 y. The assumed parameter values are $\Lambda = 1.4 \times 10^5$, $Pe = 10^2$, $\lambda_1 = 1.8$, $\lambda_2 = 1/\lambda_2 \approx 0.556$, $c = \beta = 1$, $a = 40$; concentration scales are $p_0 = 0.72$ mM, $g_0 = 0.2$ mM. The approximate solutions are as described in the text, using Eqs. (3.22) and (3.36), with $\beta = 1$, $u = v$, and $T^* = 5.65$. The solutions can be compared qualitatively to Fig. 3, but a direct comparison is not advisable, since the present figure does not show solutions of the same system.

groundwater reaction fronts, provided the second reactant is taken to be produced by secondary reactions which do not involve the primary carbon source. To be specific, we have considered the subsystem, written in partial and schematic form,

$$\begin{aligned} &O_2 + CH_2O \rightarrow CO_2, \\ &MnO_2 + CH_2O \rightarrow Mn^{2+}, \\ &O_2 + Mn^{2+} \rightarrow MnO_2; \end{aligned} \tag{4.1}$$

here the third reaction is a secondary reaction, consequent upon the production of Mn^{2+} by the action of MnO_2 in the second reaction as a TEA once O_2 has been depleted. Paradoxically, it is this Mn^{2+} which serves to take out the oxygen at the reaction front, the depletion of which is what causes the onset of the second reaction.

We have thus shown in principle that the application of classical reaction–diffusion theory to a hierarchy of groundwater redox reactions can account for the formation of sharp reaction fronts separating zones of distinct dominant TEA processes provided the front-forming reactions are fast ($\Lambda \gg 1$). A consequence of the approximate solutions which we obtain is that it allows for a simple analysis of the resulting concentration profiles. There is a clear scope for developing the model to produce multiple reaction fronts by the inclusion of additional terminal electron acceptor processes. This would allow for the prediction of the propagation of individual redox zones. Cribbin (2013) suggested that including Fe (III) reduction in this model resulted in the oxygen–Mn^{2+} and oxygen–Fe^{2+} reaction fronts coinciding.

Our analytic results are based on a pair of asymptotic assumptions: fast reaction, characterised by the dimensionless parameter $\Lambda \gg 1$, and slow dispersion, characterised by the Péclet number $Pe \gg 1$. In the context of the latter assumption, it should be pointed out that Gramling et al. (2002) showed experimentally that reaction rates are somewhat slower than might be expected, due to incomplete mixing of reactants at the pore scale. Gramling et al. found a 20% decrease in the mass of reaction product in their experiments. While this would affect our analytic results quantitatively, the effect is a relatively mild one.

In addition, Chiogna et al. (2010) showed experimentally that transverse dispersion coefficients depend on the dispersing substance, which has important consequences for field scale transport (Chiogna et al., 2011), and for isotope fractionation (LaBolle et al., 2008); this would lead in our model (for example, Eq. (3.1)) to different Péclet numbers for O_2 and Mn^{2+}; but as long as they are large, there is no difference in our analytic method, and no significant difference in our main thesis.

Whereas our theoretical results mimic the numerical results of Hunter et al. (1998), it is also the case that analytical approaches of this sort may offer a means of enhancing the efficiency of numerical codes in front-forming conditions by allowing coarser numerical discretisation in regions of slow spatial variation to be complemented by semi-analytical solutions in the vicinity of reaction fronts.

Acknowledgements

This publication has emanated from research conducted with the financial support of Science Foundation Ireland under Grant Number: SFI/09/IN.1/I2645. A. C. F. acknowledges the support of the Mathematics Applications Consortium for Science and Industry (www.macsi.ul.ie) funded by the Science Foundation Ireland mathematics initiative grant SFI/12/IA/1683.

References

Abrams, R.H., Loague, K., 2000a. A compartmentalized solute transport model for redox zones in contaminated aquifers. 1. Theory and development. Water Resour. Res. 36 (8), 2,001–2,013.

Abrams, R.H., Loague, K., 2000b. A compartmentalized solute transport model for redox zones in contaminated aquifers. 2. Field-scale simulations. Water Resour. Res. 36 (8), 2,015–2,029.

Ai, S., 2007. Traveling waves in a bioremediation model. SIAM J. Appl. Math. 68 (3), 680–693.

Beck, M., Doelman, A., Kaper, T.J., 2006. A geometric construction of traveling waves in a bioremediation model. J. Nonlinear Sci. 16, 329–349.
Chapelle, F.H., 2001. Ground-Water Microbiology and Geochemistry. John Wiley, New York.
Chiogna, G., Eberhardt, C., Grathwohl, P., Cirpka, O.A., Rolle, M., 2010. Evidence of compound-dependent hydrodynamic and mechanical transverse dispersion by multitracer laboratory experiments. Environ. Sci. Technol. 44, 688–693.
Chiogna, G., Cirpka, O.A., Grathwohl, P., Rolle, M., 2011. Relevance of local compound-specific transverse dispersion for conservative and reactive mixing in heterogeneous porous media. Water Resour. Res. 47, W07540.
Christensen, T.H., Bjerg, P.L., Banwart, S.A., Jakobsen, R., Heron, G., Albrechtsen, H.J., 2000. Characterization of redox conditions in groundwater contaminant plumes. J. Contam. Hydrol. 45 (3), 165–241.
Chu, M., Kitanidis, P.K., McCarty, P.L., 2005. Modeling microbial reactions at the plume fringe subject to transverse mixing in porous media: when can the rates of microbial reaction be assumed to be instantaneous? Water Resour. Res. 41, W06002.
Cirpka, O.A., 2010. Simplified simulation of steady state bioreactive transport with kinetic solute uptake by the biomass. Water Resour. Res. 46, W07534.
Cirpka, O.A., Valocchi, A.J., 2007. Two-dimensional concentration distribution for mixing-controlled bioreactive transport in steady state. Adv. Water Resour. 30 (6), 1,668–1,679.
Cirpka, O.A., Valocchi, A.J., 2009. "Reply to comments on two-dimensional concentration distribution for mixing-controlled bioreactive transport in steady state" by H. Shao et al. Adv. Water Resour. 32 (2), 298–301.
Cribbin, L.B., 2013. Soil Bacterial Processes and Dynamics(Ph. D. thesis) University of Limerick, Ireland.
Dewynne, J.N., Fowler, A.C., Hagan, P.S., 1993. Multiple reaction fronts in the oxidation/reduction of iron-rich uranium ores. SIAM J. Appl. Math. 53, 971–989.
Feeney, R., Schmidt, S.L., Strickholm, P., Chadam, J., Ortoleva, P., 1983. Periodic precipitation and coarsening waves: applications of the competitive particle growth model. J. Chem. Phys. 78 (3), 1,293–1,311.
Fowler, A.C., Winstanley, H.F., McGuinness, M.J., Cribbin, L.B., 2014. Oscillations in soil bacterial redox reactions. J. Theor. Biol. 342, 33–38.
Froelich, P.N., Klinkhammer, G.P., Bender, M.L., Luedtke, N.A., Heath, G.R., Cullen, D., Dauphin, P., Hammond, D., Hartman, B., Maynard, V., 1979. Early oxidation of organic matter in pelagic sediments of the eastern equatorial Atlantic: suboxic diagenesis. Geochim. Cosmochim. Acta 43 (7), 1,075–1,090.
Gálfi, L., Rácz, Z., 1988. Properties of the reaction front in an $A + B \rightarrow C$ type reaction–diffusion process. Phys. Rev. A38 (6), 3,151–3,154.
Gramling, C.M., Harvey, C.F., Meig, L.C., 2002. Reactive transport in porous media: a comparison of model prediction with laboratory visualization. Environ. Sci. Technol. 36, 2,508–2,514.
Gutierrez-Neri, M., Ham, P.A.S., Schotting, R.J., Lerner, D.N., 2009. Analytical modelling of fringe and core biodegradation in groundwater plumes. J. Contam. Hydrol. 107, 1–9.
Hagan, P.S., Polizzotti, R.S., Luckman, G., 1985. Internal oxidation of binary alloys. SIAM J. Appl. Math. 45, 956–971.
Ham, P., Schotting, R., Prommer, H., 2004. Effects of hydrodynamic dispersion on plume lengths for instantaneous bimolecular reactions. Adv. Water Resour. 27, 803–813.
Hunter, K.S., Wang, Y., Van Cappellen, P., 1998. Kinetic modeling of microbially-driven redox chemistry of subsurface environments: coupling transport, microbial metabolism and geochemistry. J. Hydrol. 209, 53–80.
Keijzer, H., van der Zee, S.E.A.T.M., Leijnse, A., 1998. Characteristic regimes for in-situ bioremediation of aquifers by injecting water containing an electron acceptor. Comput. Geosci. 2, 1–22.
Keijzer, H., van Dijke, M.I.J., van der Zee, S.E.A.T.M., 1999. Analytical approximation to characterize the performance of in situ aquifer bioremediation. Adv. Water Resour. 23, 217–228.
Keller, J.B., Rubinow, S.I., 1981. Recurrent precipitation and Liesegang rings. J. Chem. Phys. 74, 5,000–5,007.
Koza, K., Taitelbaum, H., 1996. Motion of the reaction front in the $A + B \rightarrow C$ reaction–diffusion system. Phys. Rev. E54 (2), R1040–R1043.
LaBolle, E.M., Fogg, G.E., Eweis, J.B., Gravner, J., Leaist, D.G., 2008. Isotopic fractionation by diffusion in groundwater. Water Resour. Res. 44, W07405.
Lerner, D.N., Thornton, S.F., Spence, M.J., Banwart, S.A., Bottrell, S.H., Higgo, J.J., Mallinson, H.E.H., Pickup, R.W., Williams, G.M., 2000. Ineffective natural attenuation of degradable organic compounds in a phenolcontaminated aquifer. Ground Water 38 (6), 922–928.
Liedl, R., Valocchi, A.J., Dietrich, P., Grathwohl, P., 2005. Finiteness of steady state plumes. Water Resour. Res. 41, W12501.
MacQuarrie, K.T., Sudicky, E.A., 2001. Multicomponent simulation of wastewater-derived nitrogen and carbon in shallow unconfined aquifers: I. Model formulation and performance. J. Contam. Hydrol. 47 (1), 53–84.
Murray, R.E., 2002. Oscillatory dynamics of the biologically active zone in in situ bioremediation. Water Resour. Res. 38 (10), 1203.
Nambi, I.M., Werth, C.J., Sanford, R.A., Valocchi, A.J., 2003. Pore-scale analysis of anaerobic halorespiring bacterial growth along the transverse mixing zone of an etched silicon pore network. Environ. Sci. Technol. 37, 5,617–5,624.
Oya, S., Valocchi, A.J., 1997. Characterization of traveling waves and analytical estimation of pollutant removal in one-dimensional subsurface bioremediation modeling. Water Resour. Res. 33 (5), 1,117–1,127.
Rolle, M., Clement, T.P., Sethi, R., Di Molfetta, A., 2008. A kinetic approach for simulating redox-controlled fringe and core biodegradation processes in groundwater: model development and application to a landfill site in Piedmont, Italy. Hydrol. Process. 22 (25), 4,905–4,921.
Sinder, M., Pelleg, J., 1999. Properties of the crossover from nonclassical to classical chemical kinetics in a reversible $A + B \rightarrow C$ reaction diffusion process. Phys. Rev. E60 (6), R6259–R6262.
Smits, T.H.M., Hüttmann, A., Lerner, D.N., Holliger, C., 2009. Detection and quantification of bacteria involved in aerobic and anaerobic ammonium oxidation in an ammonium-contaminated aquifer. Biorem. J. 13, 41–51.
Taitelbaum, H., Koo, Y.-E.L., Havlin, S., Kopelman, R., Weiss, G.H., 1992. Exotic behavior of the reaction front in the $A + B \rightarrow C$ reaction–diffusion system. Phys. Rev. E46 (4), 2,151–2,154.
Thullner, M., Van Cappellen, P., Regnier, P., 2005. Modeling the impact of microbial activity on redox dynamics in porous media. Geochim. Cosmochim. Acta 69 (21), 5,005–5,019.
Wang, Y., Van Cappellen, P., 1996. A multicomponent reactive transport model of early diagenesis: application to redox cycling in coastal marine sediments. Geochim. Cosmochim. Acta 60, 2,993–3,014.
Xin, J.X., Hyman, J.M., 2000. Stability, relaxation, and oscillation of biodegradation fronts. SIAM J. Appl. Math. 61 (2), 472–505.